

Deterministic Entanglement of Large-Scale Hermite-Gaussian Modes

Xutong Wang¹ and Jietai Jing^{1,2,3,4,*}

¹State Key Laboratory of Precision Spectroscopy, Joint Institute of Advanced Science and Technology, School of Physics and Electronic Science, East China Normal University, Shanghai 200062, China

²CAS Center for Excellence in Ultra-intense Laser Science, Shanghai 201800, China

³Department of Physics, Zhejiang University, Hangzhou 310027, China

⁴Collaborative Innovation Center of Extreme Optics, Shanxi University, Taiyuan, Shanxi 030006, China

(Received 22 December 2021; revised 30 June 2022; accepted 1 July 2022; published 22 August 2022)

Continuous-variable (CV) entanglement constitutes a powerful approach to deterministic quantum information protocols. Improving the scale of entanglement is of vital importance for enhancing the information capacity of quantum information protocols. Here we demonstrate the deterministic generation of CV entanglement of large-scale Hermite-Gaussian (HG) modes from the four-wave mixing (FWM) process in an atomic vapor. In our experiment, 56 pairs of entangled HG modes are deterministically and simultaneously generated from the FWM process, which increases the number of entangled spatial mode pairs in the CV system. Meanwhile, we experimentally verify the existence of CV entanglement between the evolution process from HG mode to Laguerre-Gaussian mode. Our results shed light on constructing high-capacity CV quantum information protocols and provide a promising platform to study CV entanglement.

DOI: 10.1103/PhysRevApplied.18.024057

I. INTRODUCTION

Quantum entanglement, which Einstein called “spooky action at a distance,” is an intriguing property of quantum mechanics [1] and forms the cornerstone of diverse quantum information protocols that outperform their classical counterparts [2–7]. Continuous-variable (CV) [8] and discrete-variable (DV) [9] systems are two main branches of quantum information systems and possess respective advantages. Quantum information protocols based on CV entanglement have experienced extensive development because CV quantum systems offer the advantage of deterministic generation of entanglement [8,10]. To construct large-scale quantum information protocols, multiplexing is an extremely important route. By integrating multiple channels into one, multiplexing can enhance the number of entanglements in CV system based on different types of degrees of freedom (DOFs), such as wavelength [11–14], time [15–18], and space [19,20]. Recently, orbital-angular-momentum (OAM) multiplexing has been demonstrated in CV systems [21,22], showing that the spatial mode is a promising DOF to multiplex CV entanglement. However, OAM modes are a subset of Laguerre-Gaussian (LG) modes and cannot completely describe the entire transverse mode space. To further boost the number of entangled spatial mode pairs in CV systems, it is promising to

multiplex CV entanglement by making use of a complete spatial mode set [23].

Hermite-Gaussian (HG) and LG modes are two sets of natural resonating modes in stable laser resonators [24,25]. They are solutions of the paraxial wave equation in Cartesian and cylindrical coordinates, respectively. Compared with LG modes, HG modes exhibit more resilience to atmospheric turbulence [26,27] and show self-healing property after an obstruction [28], which indicates advantages in free-space communication protocols. Meanwhile, the unique spatial characteristics of HG modes make them useful in small-displacement and tilt measurements [29], particle manipulation [30], and so on. More importantly, HG modes, which are characterized by two mode indexes n and m , provide a basis to fully represent the spatial structure of the transverse field and thus can greatly enhance the information capacity of communication systems. So far, HG modes have been employed to demonstrate entanglement in both CV [31,32] and DV [33,34] systems. However, CV entanglement between HG modes is typically generated from the optical parametric oscillator and confined to the relatively lower orders [35], which limit their application in large-scale information encoding. The four-wave mixing (FWM) process in a hot ^{85}Rb atomic vapor has been shown as a favorable resource for quantum entanglement, owing to its spatially multimode nature and strong nonlinearity without an optical cavity [20–22,36]. Therefore, it is promising to exploit higher-order HG

*Corresponding author. jtjing@phy.ecnu.edu.cn

modes from the FWM process to enhance the information capacity of CV systems.

In this paper, we utilize the FWM process in a hot ^{85}Rb atomic vapor to generate 56 pairs of HG modes. The CV entanglement between two HG modes with the same mode indexes is verified in our experiment. Our results increase the number of entangled spatial mode pairs in the CV system. Meanwhile, we experimentally demonstrate the existence of CV entanglement in the evolution process from HG mode to LG mode. Our scheme utilizing a complete spatial mode set provides an efficient way to enhance the information capacity of CV systems and can be applied to parallel quantum information processing.

II. EXPERIMENTAL RESULTS

The FWM process is based on the double- Λ energy level configuration in the $D1$ line of ^{85}Rb . Two pump photons are converted into a probe and a conjugate photon in the hot ^{85}Rb atomic vapor. Phase-matching conditions ensure that the generated probe and conjugate modes are identical in the mode indexes of HG modes. Then the interaction Hamiltonian of the FWM process can be described as

$$\hat{H} = \sum_{n,m} i\hbar\gamma_{n,m} \hat{a}_{n,m}^\dagger \hat{b}_{n,m}^\dagger + \text{H.c.}, \quad (1)$$

where $\hat{a}_{n,m}^\dagger$ and $\hat{b}_{n,m}^\dagger$ are the creation operators of probe and conjugate modes, respectively, $\gamma_{n,m}$ is the corresponding interaction strength of a pair of HG modes, and H.c. denotes the Hermitian conjugate. After applying the time-evolution operator to vacuum state, a number of independent two-mode squeezed vacuum states $|\psi\rangle_{n,m}$ are generated. The output field of the FWM process can be written as

$$|\psi\rangle_{\text{out}} = \prod_{n,m} |\psi\rangle_{n,m}. \quad (2)$$

These two-mode squeezed vacuum states are multiple pairs of simultaneously generated HG modes, i.e., CV entanglement is multiplexed in a series of orthogonal HG modes.

Figure 1(a) shows the experimental setup, where two identical FWM processes happen in the same atomic cell. The pump and probe beams of the FWM processes are produced by a Ti:sapphire laser whose frequency is stabilized at 377.1102 THz. The bright probe beam is redshifted by about 3.04 GHz via an acousto-optic modulator (AOM) and transformed into HG modes via a spatial light modulator (SLM). Then the probe beam is crossed with the strong pump beam at about 7 mrad, leading to the generation of a bright conjugate beam. Similarly, parts of the probe and

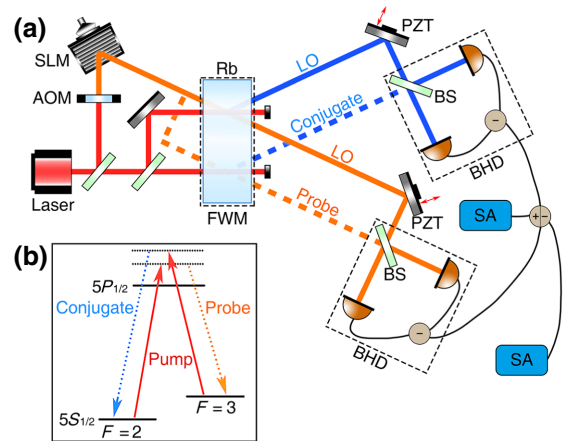


FIG. 1. Experimental scheme for deterministic generation of CV entanglement of large-scale HG modes. (a) The detailed experimental setup. (b) The energy level diagram of the double- Λ configuration in the $D1$ line of ^{85}Rb .

pump beam are split out to serve another FWM process. The images of FWM output fields captured by a charge-coupled device (CCD) for varying HG modes are shown in Fig. 2(a). In each image, the beam profiles from right to left are amplified probe beam, pump beam, and newly generated conjugate beam, respectively. With an increase of either mode index of HG mode, the beam size becomes larger, resulting in less overlap with the pump beam in the FWM process. As a result, weaker interaction strength induced by less overlap leads to smaller intensity gain, which is shown in Fig. 2(b).

The positivity under partial transposition (PPT) criterion [37] is widely employed in CV systems to verify entanglement. One can characterize the entanglement properties by constructing the covariance matrix (CM) from the amplitude and phase quadratures and calculating the smallest symplectic eigenvalue v of the partially transposed CM. An entangled state is verified if and only if v is smaller than 1 for the bipartite case. In our system, the CM for $\text{HG}_{n,m}$ modes can be expressed as $\sigma_{n,m} = \langle \xi^T \xi \rangle$, where $\xi = (\hat{X}_{n,m}^{\text{Pr}}, \hat{Y}_{n,m}^{\text{Pr}}, \hat{X}_{n,m}^{\text{Conj}}, \hat{Y}_{n,m}^{\text{Conj}})$. $\hat{X}_{n,m}^{\text{Pr}} (\hat{Y}_{n,m}^{\text{Pr}})$ and $\hat{X}_{n,m}^{\text{Conj}} (\hat{Y}_{n,m}^{\text{Conj}})$ are the amplitude (phase) quadratures of the probe and conjugate fields, respectively. Two balanced homodyne detections (BHDs) are used to project the output field of the FWM process onto the same HG mode using two local oscillators (LOs) and to measure the elements of the CM. One BHD is used for detecting the probe fields and the other for the conjugate field. We block the probe beam of one FWM process, making it an unseeded FWM process. Such an unseeded FWM process is used for the generation of entangled HG modes as represented in Eq. (2), while the seeded FWM process is used for generating the LOs of the two BHDs. The desired field quadrature can be measured by employing two scanned piezoelectric

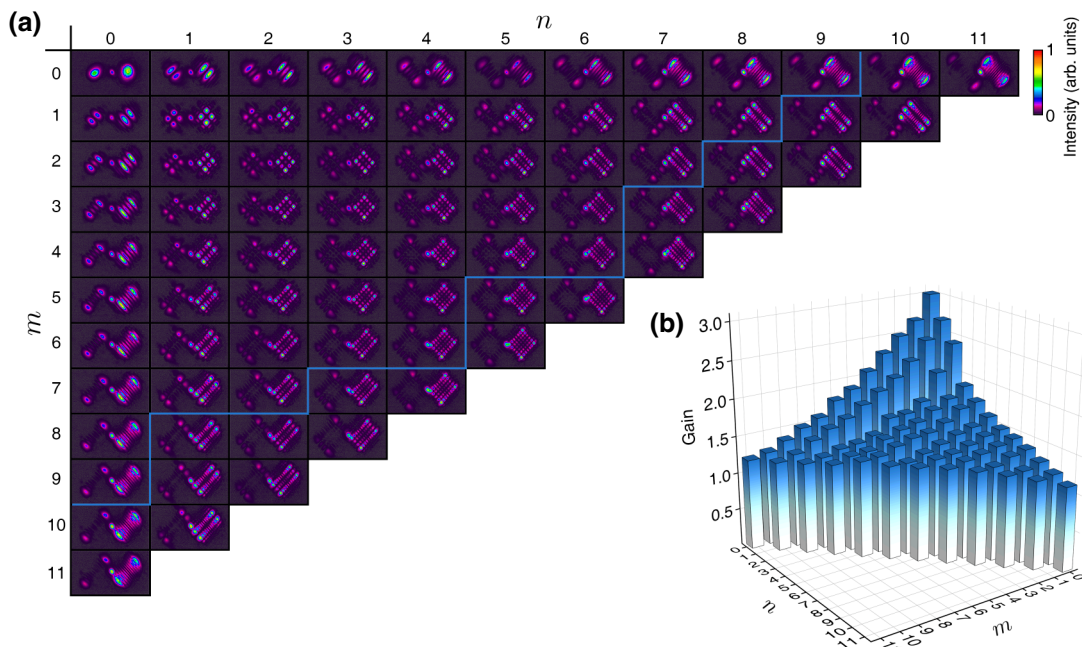


FIG. 2. Images and intensity gain of entangled HG modes. (a) CCD-captured images of HG modes with varying indexes generated from the FWM process. Labeled columns represent the index m of the probe beam, while labeled rows represent the index n of the probe beam. The beam profiles from right to left in each image are amplified probe beam, pump beam, and newly generated conjugate beam, respectively. (b) Intensity gain as a function of the two indexes n and m .

transducers (PZTs) to change the phases of the two BHDs. Then we can obtain the variance of the single-field quadrature according to the photocurrent from each BHD, and the covariance of the two-field quadrature is given by the photocurrent from two BHDs and their subtraction or addition. These photocurrents are recorded by two spectrum analyzers (SAs), which are set to 1.5-MHz center

frequency. After constructing the CMs for different HG modes, the corresponding ν is shown in Fig. 3. With an increase of either mode index n or m , ν increases, indicating the reduction of the degree of CV entanglement. For higher-order HG modes, CV entanglement disappears when ν is not smaller than 1, due to weak nonlinear interaction strength. The entangled modes are colored in Fig. 3 [they are also marked inside the blue frame in Fig. 2(a)]. Such results show consistency with Fig. 2(b) because in our system ν is a function of intensity gain (see Appendix B), and ν increases with the decrease of intensity gain. In theory, HG modes always stay entangled when the corresponding intensity gain is greater than 1. However, there are inevitable losses in experimental implementation, which give rise to excess noise. Under our experimental conditions, we achieve a maximal range of n and m from 0 to 9 for entanglement generation. With an increase of either index, the range of the other index possessing entanglement gets smaller, for the reason that the beam waist of the HG mode is proportional to $\sqrt{n+m+1}$. Altogether, 56 pairs of entangled HG modes are deterministically generated from the FWM process, indicating the large information capacity of the system.

Further, it is interesting to investigate CV entanglement between a more generalized mode set [38,39]

$$u_{n,m}(x,y,z) = \sum_{k=0}^N e^{iCk} b(n,m,k) u_{N-k,k}^{\text{HG}}(x,y,z), \quad (3)$$

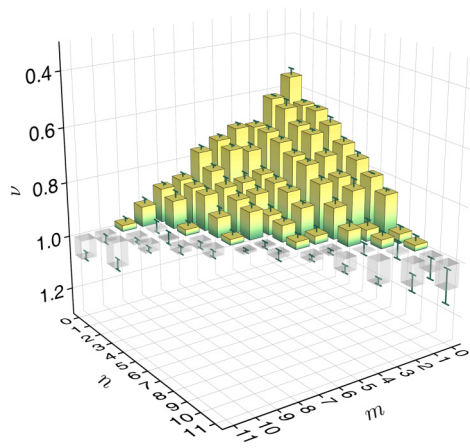


FIG. 3. The smallest symplectic eigenvalue ν of the partially transposed CM as a function of the two indexes n and m . The colored pillars represent entangled modes. All these results are uncorrected for the detection efficiency. The uncertainties are statistical, one standard deviation of multiple repeated measurements.

where

$$b(n, m, k) = \left(\frac{(N - k)!k!}{2^N n!m!} \right)^{1/2} \frac{1}{k!} \frac{d^k}{dt^k} [(1-t)^n(1+t)^m]_{t=0}, \quad (4)$$

$u_{n,m}^{\text{HG}}(x, y, z)$ is the complex amplitude of HG modes, $N = n + m$ is defined as the order of the modes, and C is a constant. These series of modes can be seen as the superposition of HG modes with the same order N . When $C = \pi/2$, Eq. (3) represents the widely used LG mode; when $C = 0$, it represents a diagonal HG mode whose coordinate axes make an angle of 45° in the (x, y) plane with the Cartesian coordinates (diagonal HG mode is used in entanglement generation and verification experiment mentioned above because it has the same characteristic as HG mode); when C is in the range from 0 to $\pi/2$, it represents the evolution process from HG mode to LG mode. For any fixed C , Eq. (3) constitutes a mode set meeting both orthogonality and completeness. To investigate the CV entanglement property in the gradual evolution process from HG mode to LG mode, we focus on several particular cases with C varying from 0 to $\pi/2$ when $n = 1$ and $m = 3$. In such a

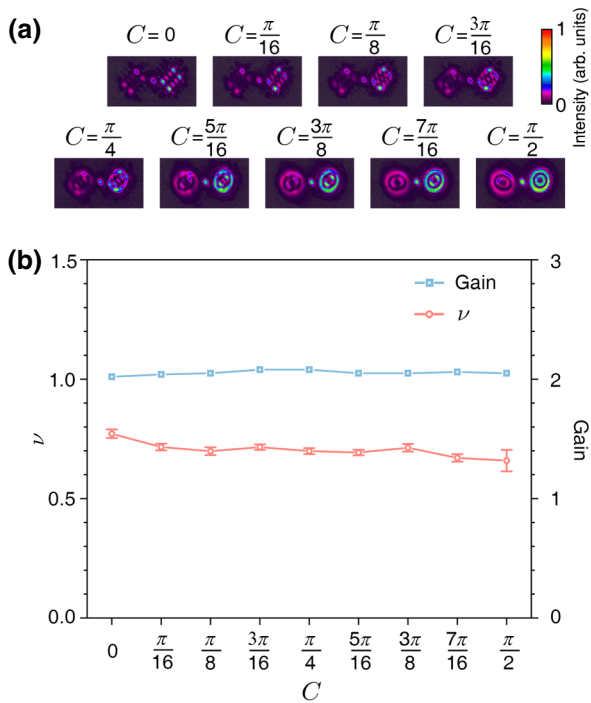


FIG. 4. Entanglement evolution from HG mode to LG mode. (a) CCD-captured images from the FWM process for different values of constant C . (b) Intensity gain (blue square) and the smallest symplectic eigenvalue ν of the partially transposed CM (red circle) as a function of the constant C . All these results are uncorrected for the detection efficiency. The uncertainties are statistical, one standard deviation of multiple repeated measurements.

process, diagonal $\text{HG}_{1,3}$ mode is gradually evolved into $\text{LG}_{1,2}$ mode (for $\text{LG}_{p,\ell}$ mode, p is the radial index and ℓ is the topological charge which corresponds to the OAM of the optical field). The output images of the FWM process for different C are shown in Fig. 4(a), which displays the mode evolution in both probe and conjugate beams. Note that the topological charges of the probe and conjugate beams are opposite due to OAM conservation in the FWM process. In a similar way to HG modes, the intensity gain (blue square) and the smallest symplectic eigenvalue ν of the partially transposed CM (red circle) as a function of C are measured and shown in Fig. 4(b). For C from 0 to $\pi/2$, ν is always smaller than 1, indicating the existence of entanglement in the evolution process. These modes are of the same order with the same beam waist, resulting in similar nonlinear interaction strength, which explains that the intensity gain and ν for these modes are almost the same. Therefore, any orthogonal spatial mode set, which is not limited to conventional HG or LG mode, can be used to exploit multiplexing in CV systems as long as these sets are orthogonal. One can choose any set according to whether it is convenient for implementation in practical applications. For example, compared with the robustness of HG modes in free-space information transmission [26–28], LG modes are widely used in fiber-based communication systems such as OAM mode division multiplexing in fibers [40] and propagation stability of radial modes in graded-index fibers [41].

III. CONCLUSION AND DISCUSSION

In conclusion, we make full use of the spatial DOFs by multiplexing CV entanglement in HG modes. In our experiment, 56 pairs of entangled HG modes are deterministically and simultaneously generated from the FWM process in a hot ^{85}Rb atomic vapor. In addition, we demonstrate the entanglement between the evolution process from HG modes to LG modes. Compared with previous works on spatial mode multiplexing in CV systems, our demonstration increases the number of entangled spatial mode pairs and provides an efficient way to enhance the information capacity of CV systems. Utilizing HG mode sorting [42–44], these HG modes can be efficiently spatially separated, which may find applications in building distant quantum communication networks. For high-speed manipulation of spatial modes in future quantum computing applications, several approaches [45–48] can be adopted. Note that our results feature CV hyperentanglement [49, 50] because the two mode indexes of HG modes provide two independent spatial DOFs. Our current implementation is only limited to spatial DOFs. It is promising to combine spatial mode multiplexing with other multiplexing technologies [11–18] to further develop larger-scale CV entanglement and give full play to the advantages of each DOF to address diverse requirements in quantum

information processing. Applying classical data postprocessing [51] to our multimode quantum resource may realize the generation of genuine multipartite entanglement analogy with the demonstration using frequency DOF [52]. Our results shed light on developing high-capacity CV quantum information protocols and provide a promising platform to study CV entanglement.

ACKNOWLEDGMENTS

This work is funded by Innovation Program of Shanghai Municipal Education Commission (Grant No. 2021-01-07-00-08-E00100); the National Natural Science Foundation of China (Grants No. 11874155, No. 91436211, No. 11374104, and No. 12174110); Basic Research Project of Shanghai Science and Technology Commission (Grant No. 20JC1416100); Natural Science Foundation of Shanghai (Grant No. 17ZR1442900); Minhang Leading Talents (Grant No. 201971); Shanghai Sailing Program (Grant No. 21YF1410800); Shanghai Municipal Science and Technology Major Project (Grant No. 2019SHZDZX01); and the 111 project (Grant No. B12024).

APPENDIX A: THE FUNDAMENTAL CHARACTERISTICS OF HG MODE

The electric field representation of HG mode is given by

$$\begin{aligned} u_{n,m}^{\text{HG}}(x,y,z) &= \sqrt{\frac{2}{\pi n!m!}} \frac{2^{-(n+m)/2}}{\omega} \exp\left(-\frac{x^2+y^2}{\omega^2}\right) \\ &\quad \times \exp\left[-i\frac{k(x^2+y^2)}{2R}\right] \\ &\quad \times H_n\left(\frac{\sqrt{2}x}{\omega}\right) H_m\left(\frac{\sqrt{2}y}{\omega}\right) \\ &\quad \times \exp\left[-i(n+m+1)\arctan\frac{z}{z_R}\right], \end{aligned} \quad (\text{A1})$$

with

$$Z_R = \frac{1}{2}k\omega^2(0), \quad (\text{A2})$$

$$R(z) = \frac{z^2+z_R^2}{z}, \quad (\text{A3})$$

$$\frac{1}{2}k\omega^2(z) = \frac{z^2+z_R^2}{z_R}, \quad (\text{A4})$$

where $H_n(x)$ is the Hermite polynomial of order n and k is the wave number. HG modes have the following orthogonality:

$$\begin{aligned} &\int_0^\infty \int_0^\infty u_{n_1,m_1}^{\text{HG}}(x,y) u_{n_2,m_2}^{\text{HG}*}(x,y) dx dy \\ &= \delta_{n_1,n_2} \delta_{m_1,m_2}. \end{aligned} \quad (\text{A5})$$

The two indexes n and m are independent in mode orthogonality, which indicates that they can provide two independent spatial DOFs.

APPENDIX B: THE THEORETICAL MODEL

Labeling the creation operators of $\text{HG}_{n,m}^{\text{Pr}}$ and $\text{HG}_{n,m}^{\text{Conj}}$ modes as $\hat{a}_{n,m}^\dagger$ and $\hat{b}_{n,m}^\dagger$, respectively, and denoting the strength of the interaction with each pair of HG modes as the real parameter $\gamma_{n,m}$, the interaction Hamiltonian of the FWM process can be written as

$$\hat{H} = \sum_{n,m} i\hbar\gamma_{n,m} \hat{a}_{n,m}^\dagger \hat{b}_{n,m}^\dagger + \text{H.c.}, \quad (\text{B1})$$

in which H.c. denotes the Hermitian conjugate. Then the corresponding time-evolution operator can be expressed as

$$\hat{U}(t) = e^{-i\hat{H}t/\hbar} = e^{\sum_{n,m} \gamma_{n,m} (\hat{a}_{n,m}^\dagger \hat{b}_{n,m}^\dagger - \hat{a}_{n,m} \hat{b}_{n,m}) t}. \quad (\text{B2})$$

Using the commutation relations

$$\begin{aligned} [\hat{a}_{n_1,m_1}, \hat{a}_{n_2,m_2}^\dagger] &= [\hat{b}_{n_1,m_1}, \hat{b}_{n_2,m_2}^\dagger] = \delta_{n_1,n_2} \delta_{m_1,m_2}, \\ [\hat{a}_{n_1,m_1}, \hat{a}_{n_2,m_2}] &= [\hat{a}_{n_1,m_1}^\dagger, \hat{a}_{n_2,m_2}^\dagger] = [\hat{b}_{n_1,m_1}, \hat{b}_{n_2,m_2}] \\ &= [\hat{b}_{n_1,m_1}^\dagger, \hat{b}_{n_2,m_2}^\dagger] = [\hat{a}_{n_1,m_1}, \hat{b}_{n_2,m_2}] = [\hat{a}_{n_1,m_1}^\dagger, \hat{b}_{n_2,m_2}^\dagger] \\ &= [\hat{a}_{n_1,m_1}, \hat{b}_{n_2,m_2}^\dagger] = [\hat{b}_{n_1,m_1}, \hat{a}_{n_2,m_2}^\dagger] = 0 \end{aligned} \quad (\text{B3})$$

and the Baker-Hausdorff theorem

$$e^{\hat{A}+\hat{B}} = e^{\hat{A}} e^{\hat{B}} e^{[\hat{A},\hat{B}]/2}, \quad (\text{B4})$$

the time-evolution operator can be further written as

$$\begin{aligned} \hat{U}(t) &= e^{\sum_{n,m} \gamma_{n,m} (\hat{a}_{n,m}^\dagger \hat{b}_{n,m}^\dagger - \hat{a}_{n,m} \hat{b}_{n,m}) t} \\ &= \prod_{n,m} e^{\gamma_{n,m} (\hat{a}_{n,m}^\dagger \hat{b}_{n,m}^\dagger - \hat{a}_{n,m} \hat{b}_{n,m}) t}. \end{aligned} \quad (\text{B5})$$

Then by applying the time-evolution operator to the vacuum state, the state of the FWM output field can be written as

$$\begin{aligned} |\psi\rangle_{\text{out}} &= \hat{U}(t)|\text{vac}\rangle \\ &= \prod_{n,m} e^{\gamma_{n,m} (\hat{a}_{n,m}^\dagger \hat{b}_{n,m}^\dagger - \hat{a}_{n,m} \hat{b}_{n,m}) t} |\text{vac}\rangle. \end{aligned} \quad (\text{B6})$$

Supposing that the mixing interaction occurs over a timescale τ , the time-evolution operator can be

described as

$$\begin{aligned}\hat{U}(\tau) &= \prod_{n,m} e^{\gamma_{n,m}(\hat{a}_{n,m}^\dagger \hat{b}_{n,m}^\dagger - \hat{a}_{n,m} \hat{b}_{n,m})\tau} \\ &= \prod_{n,m} U_{n,m}(\tau).\end{aligned}\quad (\text{B7})$$

Then we set

$$\hat{S}(r_{n,m}) \equiv U_{n,m}(\tau) = e^{r_{n,m}(\hat{a}_{n,m}^\dagger \hat{b}_{n,m}^\dagger - \hat{a}_{n,m} \hat{b}_{n,m})}, \quad (\text{B8})$$

which is the so-called two-mode squeezing operator squeezing the modes $\hat{a}_{n,m}$ and $\hat{b}_{n,m}$ together, and $r_{n,m} = \gamma_{n,m}\tau$ is the squeezing parameter quantifying the degree of mixing. Then the final state of the FWM output field can be further written as

$$|\psi\rangle_{\text{out}} = \prod_{n,m} \hat{S}(r_{n,m}) |\text{vac}\rangle_{n,m} = \prod_{n,m} |\psi\rangle_{n,m}, \quad (\text{B9})$$

where $\hat{S}(r_{n,m})$ are a series of two-mode squeezing operators corresponding to independent two-mode squeezing vacuum states $|\psi\rangle_{n,m}$. As can be seen, these two-mode squeezed vacuum states are independent HG modes, which means that CV entanglement multiplexed in HG modes can be generated from the FWM process.

Each pair of generated HG modes can be described quantum mechanically by corresponding amplitude and phase quadratures. In our system, they can be written as

$$\begin{aligned}\hat{X}_{n,m}^{\text{Pr}} &= \frac{\hat{a}_{n,m} + \hat{a}_{n,m}^\dagger}{\sqrt{2}}, & \hat{Y}_{n,m}^{\text{Pr}} &= \frac{\hat{a}_{n,m} - \hat{a}_{n,m}^\dagger}{\sqrt{2}i}, \\ \hat{X}_{n,m}^{\text{Conj}} &= \frac{\hat{b}_{n,m} + \hat{b}_{n,m}^\dagger}{\sqrt{2}}, & \hat{Y}_{n,m}^{\text{Conj}} &= \frac{\hat{b}_{n,m} - \hat{b}_{n,m}^\dagger}{\sqrt{2}i}.\end{aligned}\quad (\text{B10})$$

Then we can construct the corresponding CM $\sigma_{n,m}$ to characterize the quantum property of each pair of HG modes:

$$\sigma_{n,m} = \begin{bmatrix} \langle \hat{X}_{n,m}^{\text{Pr}} \hat{X}_{n,m}^{\text{Pr}} \rangle & \langle \hat{X}_{n,m}^{\text{Pr}} \hat{Y}_{n,m}^{\text{Pr}} \rangle & \langle \hat{X}_{n,m}^{\text{Pr}} \hat{X}_{n,m}^{\text{Conj}} \rangle & \langle \hat{X}_{n,m}^{\text{Pr}} \hat{Y}_{n,m}^{\text{Conj}} \rangle \\ \langle \hat{Y}_{n,m}^{\text{Pr}} \hat{X}_{n,m}^{\text{Pr}} \rangle & \langle \hat{Y}_{n,m}^{\text{Pr}} \hat{Y}_{n,m}^{\text{Pr}} \rangle & \langle \hat{Y}_{n,m}^{\text{Pr}} \hat{X}_{n,m}^{\text{Conj}} \rangle & \langle \hat{Y}_{n,m}^{\text{Pr}} \hat{Y}_{n,m}^{\text{Conj}} \rangle \\ \langle \hat{X}_{n,m}^{\text{Conj}} \hat{X}_{n,m}^{\text{Pr}} \rangle & \langle \hat{X}_{n,m}^{\text{Conj}} \hat{Y}_{n,m}^{\text{Pr}} \rangle & \langle \hat{X}_{n,m}^{\text{Conj}} \hat{X}_{n,m}^{\text{Conj}} \rangle & \langle \hat{X}_{n,m}^{\text{Conj}} \hat{Y}_{n,m}^{\text{Conj}} \rangle \\ \langle \hat{Y}_{n,m}^{\text{Conj}} \hat{X}_{n,m}^{\text{Pr}} \rangle & \langle \hat{Y}_{n,m}^{\text{Conj}} \hat{Y}_{n,m}^{\text{Pr}} \rangle & \langle \hat{Y}_{n,m}^{\text{Conj}} \hat{X}_{n,m}^{\text{Conj}} \rangle & \langle \hat{Y}_{n,m}^{\text{Conj}} \hat{Y}_{n,m}^{\text{Conj}} \rangle \end{bmatrix}. \quad (\text{B11})$$

According to

$$\hat{S}^\dagger(r_{n,m}) = \hat{S}^{-1}(r_{n,m}) = \hat{S}(r_{n,m}) \quad (\text{B12})$$

and

$$e^{\hat{A}} \hat{B} e^{-\hat{A}} = \sum_{i=0}^{\infty} \frac{1}{i!} [\hat{A}^{(i)}, \hat{B}], \quad (\text{B13})$$

the unitary transformation properties of two-mode squeezing operator can be obtained:

$$\begin{aligned}\hat{S}^\dagger(r_{n,m}) \hat{X}_{n,m}^{\text{Pr}} \hat{S}(r_{n,m}) &= \hat{X}_{n,m}^{\text{Pr}} \cosh(r_{n,m}) + \hat{X}_{n,m}^{\text{Conj}} \sinh(r_{n,m}), \\ \hat{S}^\dagger(r_{n,m}) \hat{X}_{n,m}^{\text{Conj}} \hat{S}(r_{n,m}) &= \hat{X}_{n,m}^{\text{Conj}} \cosh(r_{n,m}) + \hat{X}_{n,m}^{\text{Pr}} \sinh(r_{n,m}),\end{aligned}$$

$$\begin{aligned}\hat{S}^\dagger(r_{n,m}) \hat{Y}_{n,m}^{\text{Pr}} \hat{S}(r_{n,m}) &= \hat{Y}_{n,m}^{\text{Pr}} \cosh(r_{n,m}) + \hat{Y}_{n,m}^{\text{Conj}} \sinh(r_{n,m}), \\ \hat{S}^\dagger(r_{n,m}) \hat{Y}_{n,m}^{\text{Conj}} \hat{S}(r_{n,m}) &= \hat{Y}_{n,m}^{\text{Conj}} \cosh(r_{n,m}) + \hat{Y}_{n,m}^{\text{Pr}} \sinh(r_{n,m}).\end{aligned}\quad (\text{B14})$$

Then the element of the CM can be calculated:

$$\begin{aligned}\langle \hat{X}_{n,m}^{\text{Pr}} \hat{X}_{n,m}^{\text{Pr}} \rangle &= {}_{n,m} \langle \psi | \hat{X}_{n,m}^{\text{Pr}} \hat{X}_{n,m}^{\text{Pr}} | \psi \rangle_{n,m} \\ &= \langle \text{vac} | \hat{S}^\dagger(r_{n,m}) \hat{X}_{n,m}^{\text{Pr}} \hat{S}(r_{n,m}) \hat{S}^\dagger(r_{n,m}) \hat{X}_{n,m}^{\text{Pr}} \\ &\quad \times \hat{S}(r_{n,m}) | \text{vac} \rangle = 2G_{n,m} - 1,\end{aligned}\quad (\text{B15})$$

where $G_{n,m} = \cosh^2(r_{n,m})$ is the intensity gain of the corresponding HG mode. Similarly all the elements of the CM can be calculated:

$$\sigma_{n,m} = \begin{bmatrix} 2G_{n,m} - 1 & 0 & 2\sqrt{G_{n,m}(G_{n,m} - 1)} & 0 \\ 0 & 2G_{n,m} - 1 & 0 & -2\sqrt{G_{n,m}(G_{n,m} - 1)} \\ 2\sqrt{G_{n,m}(G_{n,m} - 1)} & 0 & 2G_{n,m} - 1 & 0 \\ 0 & -2\sqrt{G_{n,m}(G_{n,m} - 1)} & 0 & 2G_{n,m} - 1 \end{bmatrix}. \quad (\text{B16})$$

In our system, the smallest symplectic eigenvalue $\nu_{n,m}$ of the partially transposed CM can be written as

$$\nu_{n,m} = \min[\text{Eigenvalue}(iSM\sigma_{n,m}M)] = \sqrt{1 + 8G_{n,m}(G_{n,m} - 1) - 4\sqrt{G_{n,m}(G_{n,m} - 1)(2G_{n,m} - 1)^2}}, \quad (\text{B17})$$

where

$$S = \begin{bmatrix} 0 & 1 & 0 & 0 \\ -1 & 0 & 0 & 0 \\ 0 & 0 & 0 & 1 \\ 0 & 0 & -1 & 0 \end{bmatrix}, \quad M = \begin{bmatrix} 1 & 0 & 0 & 0 \\ 0 & 1 & 0 & 0 \\ 0 & 0 & 1 & 0 \\ 0 & 0 & 0 & -1 \end{bmatrix}. \quad (\text{B18})$$

It can be seen that $\nu_{n,m}$ is smaller than 1 when corresponding $G_{n,m}$ is greater than 1, which indicates the existence of CV entanglement according to the PPT criterion.

APPENDIX C: BHD FOR HG MODE

In order to experimentally test the entanglement between HG modes, we have to extract the desired HG mode from the whole optical field and measure the corresponding CM.

The BHD technique, in which the whole optical field is projected onto a specific mode according to the tailored LO, is widely used in CV systems for its high detection efficiency. Regarding HG modes, the BHD scheme is illustrated in Fig. 5. A LO $\hat{a}u_{n_1,m_1}^{\text{HG}}(x,y)$ and a signal field $\hat{b}u_{n_2,m_2}^{\text{HG}}(x,y)$ are incident into the two ports of a 50:50 beam splitter, respectively, and then the fields of two output ports can be written as

$$\begin{aligned} \hat{c} &= \frac{1}{\sqrt{2}}[\hat{a}u_{n_1,m_1}^{\text{HG}}(x,y)e^{i\theta} + \hat{b}u_{n_2,m_2}^{\text{HG}}(x,y)], \\ \hat{d} &= \frac{1}{\sqrt{2}}[\hat{a}u_{n_1,m_1}^{\text{HG}}(x,y)e^{i\theta} - \hat{b}u_{n_2,m_2}^{\text{HG}}(x,y)], \end{aligned} \quad (\text{C1})$$

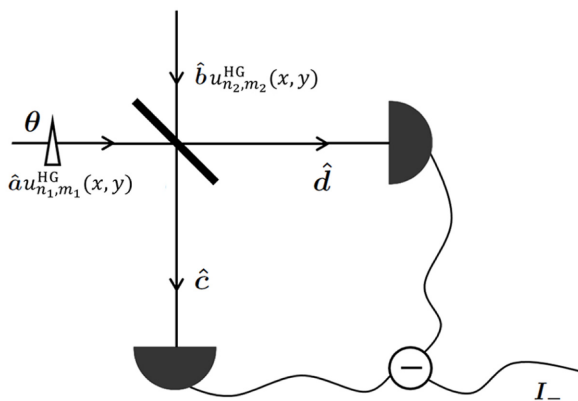


FIG. 5. Schematic of BHD for HG mode. A local oscillator and a signal field are incident into the two ports of a 50:50 beam splitter. Then the fields of two output ports are detected by two photodiodes whose photocurrents are subtracted by a subtractor.

where θ is the relative phase difference between LO and signal field. Then the fields \hat{c} and \hat{d} are detected by two photodiodes, after which the two detected photocurrents are subtracted by a subtractor. We express \hat{a} and \hat{b} as

$$\begin{aligned} \hat{a} &\approx |\alpha| + \delta\hat{a}, \\ \hat{b} &\approx |\beta| + \delta\hat{b}, \end{aligned} \quad (\text{C2})$$

and neglect terms without $|\alpha|$ because the coherence amplitude of the LO is much larger than that of the signal field ($|\alpha| \gg |\beta|$). Then the difference photocurrent can be expressed as

$$\begin{aligned} I_- &= \int_0^\infty \int_0^\infty (\hat{d}^\dagger \hat{d} - \hat{c}^\dagger \hat{c}) dx dy \\ &\propto (\hat{a}^\dagger \hat{b} e^{-i\theta} + \hat{b}^\dagger \hat{a} e^{i\theta}) \\ &\times \int_0^\infty \int_0^\infty u_{n_1,m_1}^{\text{HG}}(x,y) u_{n_2,m_2}^{\text{HG}*}(x,y) dx dy \\ &\propto |\alpha| \delta X_b^\theta \delta_{n_1,n_2} \delta_{m_1,m_2}, \end{aligned} \quad (\text{C3})$$

where $\delta X_b^\theta = \delta b e^{-i\theta} + \delta \hat{b}^\dagger e^{i\theta}$ is the amplitude quadrature of the signal field. It can be seen that the difference photocurrent is proportional to the quantum fluctuation of a specific HG mode that has the same indexes as the LO.

In our experiment, the probe and conjugate beams are detected by two sets of BHDs, respectively. Then the normalized diagonal terms of the CM can be obtained by

$$\begin{aligned} \langle \hat{X}_{n,m}^{\text{Pr}} \hat{X}_{n,m}^{\text{Pr}} \rangle &= \frac{\Delta^2(L_{n,m}^{\text{Pr}} \hat{X}_{n,m}^{\text{Pr}})}{\Delta^2(L_{n,m}^{\text{Pr}} \hat{X}_{\text{vac}})}, \\ \langle \hat{Y}_{n,m}^{\text{Pr}} \hat{Y}_{n,m}^{\text{Pr}} \rangle &= \frac{\Delta^2(L_{n,m}^{\text{Pr}} \hat{Y}_{n,m}^{\text{Pr}})}{\Delta^2(L_{n,m}^{\text{Pr}} \hat{Y}_{\text{vac}})}, \\ \langle \hat{X}_{n,m}^{\text{Conj}} \hat{X}_{n,m}^{\text{Conj}} \rangle &= \frac{\Delta^2(L_{n,m}^{\text{Conj}} \hat{X}_{n,m}^{\text{Conj}})}{\Delta^2(L_{n,m}^{\text{Conj}} \hat{X}_{\text{vac}})}, \\ \langle \hat{Y}_{n,m}^{\text{Conj}} \hat{Y}_{n,m}^{\text{Conj}} \rangle &= \frac{\Delta^2(L_{n,m}^{\text{Conj}} \hat{Y}_{n,m}^{\text{Conj}})}{\Delta^2(L_{n,m}^{\text{Conj}} \hat{Y}_{\text{vac}})}, \end{aligned} \quad (\text{C4})$$

where $\hat{X}_{n,m}^{\text{Pr}}$ ($\hat{X}_{n,m}^{\text{Conj}}$) and $\hat{Y}_{n,m}^{\text{Pr}}$ ($\hat{Y}_{n,m}^{\text{Conj}}$) are the amplitude quadrature and phase quadrature of probe (conjugate) beam, respectively, $L_{n,m}^{\text{Pr}}$ ($L_{n,m}^{\text{Conj}}$) is the optical power of the LO, $\Delta^2(L_{n,m}^{\text{Pr}} \hat{X}_{n,m}^{\text{Pr}})$ [$\Delta^2(L_{n,m}^{\text{Conj}} \hat{X}_{n,m}^{\text{Conj}})$] is the noise power of

photocurrent when the signal field is fed into the detectors, and $\Delta^2(L_{n,m}^{\text{Pr}} \hat{X}_{\text{vac}})$ [$\Delta^2(L_{n,m}^{\text{Conj}} \hat{Y}_{\text{vac}})$] is the noise power of photocurrent when the signal field is blocked. By combining the photocurrents of two BHDs via an adder (subtractor), we can measure the noise power of the sum (difference) of the two photocurrents, and the minimum of the measurement result is equal to $\Delta^2(L_{n,m}^{\text{Pr}} \hat{Y}_{n,m}^{\text{Pr}} + L_{n,m}^{\text{Conj}} \hat{Y}_{n,m}^{\text{Conj}})$ [$\Delta^2(L_{n,m}^{\text{Pr}} \hat{X}_{n,m}^{\text{Pr}} - L_{n,m}^{\text{Conj}} \hat{X}_{n,m}^{\text{Conj}})$]. Then we can obtain

$$\langle \hat{X}_{n,m}^{\text{Pr}} \hat{X}_{n,m}^{\text{Conj}} \rangle = \frac{\Delta^2(L_{n,m}^{\text{Pr}} \hat{X}_{n,m}^{\text{Pr}}) + \Delta^2(L_{n,m}^{\text{Conj}} \hat{X}_{n,m}^{\text{Conj}})}{2\sqrt{\Delta^2(L_{n,m}^{\text{Pr}} \hat{X}_{\text{vac}})}\sqrt{\Delta^2(L_{n,m}^{\text{Conj}} \hat{X}_{\text{vac}})}} - \frac{\Delta^2(L_{n,m}^{\text{Pr}} \hat{X}_{n,m}^{\text{Pr}} - L_{n,m}^{\text{Conj}} \hat{X}_{n,m}^{\text{Conj}})}{2\sqrt{\Delta^2(L_{n,m}^{\text{Pr}} \hat{X}_{\text{vac}})}\sqrt{\Delta^2(L_{n,m}^{\text{Conj}} \hat{X}_{\text{vac}})}}. \quad (\text{C5})$$

In a similar way, all the normalized off-diagonal terms of the CM can be obtained. Then we can fully construct the CM for characterizing CV entanglement.

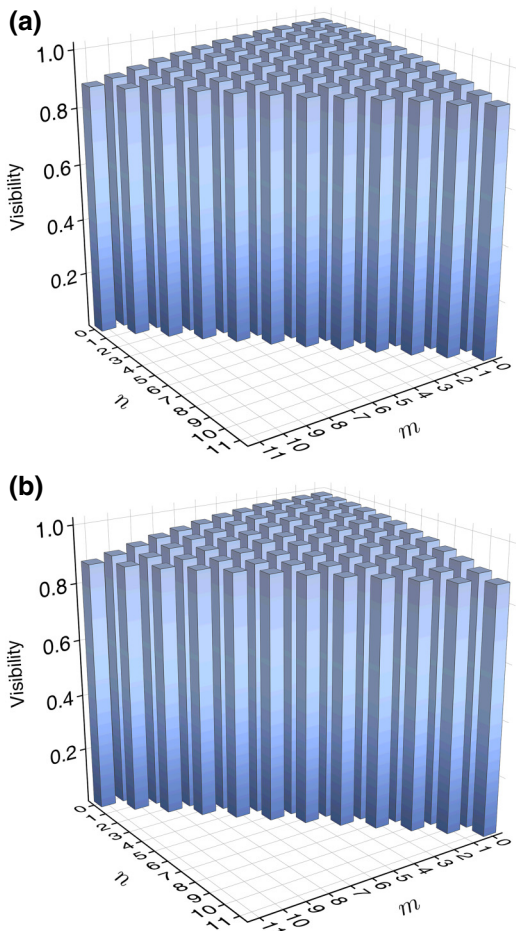


FIG. 6. Interference visibilities of the BHDs for detecting the (a) probe and (b) conjugate fields as a function of the two mode indexes.

The extraction efficiency of the BHD depends on the interference visibility between the LO and signal field. We can record the visibilities between the corresponding LO and probe (conjugate) fields by making the two FWM interactions identical. The results are illustrated in Fig. 6. These visibilities are within the range of 0.88 and 0.98 and decrease slightly with an increase of the two indexes, indicating the high extraction efficiency of HG modes.

-
- [1] R. Horodecki, P. Horodecki, M. Horodecki, and K. Horodecki, Quantum entanglement, *Rev. Mod. Phys.* **81**, 865 (2009).
 - [2] S. Wengerowsky, S. K. Joshi, F. Steinlechner, H. Hübel, and R. Ursin, An entanglement-based wavelength-multiplexed quantum communication network, *Nature* **564**, 225 (2018).
 - [3] X. Guo, C. R. Breum, J. Borregaard, S. Izumi, M. V. Larsen, T. Gehring, M. Christandl, J. S. Neergaard-Nielsen, and U. L. Andersen, Distributed quantum sensing in a continuous-variable entangled network, *Nat. Phys.* **16**, 281 (2020).
 - [4] H.-S. Zhong, *et al.*, Quantum computational advantage using photons, *Science* **370**, 1460 (2020).
 - [5] J. M. Arrazola, *et al.*, Quantum circuits with many photons on a programmable nanophotonic chip, *Nature* **591**, 54 (2021).
 - [6] L.-Z. Liu, Y.-Z. Zhang, Z.-D. Li, R. Zhang, X.-F. Yin, Y.-Y. Fei, L. Li, N.-L. Liu, F. Xu, Y.-A. Chen, and J.-W. Pan, Distributed quantum phase estimation with entangled photons, *Nat. Photon.* **15**, 137 (2021).
 - [7] M. Pompili, S. L. N. Hermans, S. Baier, H. K. C. Beukers, P. C. Humphreys, R. N. Schouten, R. F. L. Vermeulen, M. J. Tiggelman, L. dos Santos Martins, B. Dirkse, S. Wehner, and R. Hanson, Realization of a multinode quantum network of remote solid-state qubits, *Science* **372**, 259 (2021).
 - [8] S. L. Braunstein and P. van Loock, Quantum information with continuous variables, *Rev. Mod. Phys.* **77**, 513 (2005).
 - [9] J. Pan, Z. B. Chen, C. Y. Lu, H. Weinfurter, A. Zeilinger, and M. Zukowski, Multiphoton entanglement and interferometry, *Rev. Mod. Phys.* **84**, 777 (2012).
 - [10] C. Weedbrook, S. Pirandola, R. García-Patrón, N. J. Cerf, T. C. Ralph, J. H. Shapiro, and S. Lloyd, Gaussian quantum information, *Rev. Mod. Phys.* **84**, 621 (2012).
 - [11] M. Chen, N. C. Menicucci, and O. Pfister, Experimental Realization of Multipartite Entanglement of 60 Modes of a Quantum Optical Frequency Comb, *Phys. Rev. Lett.* **112**, 120505 (2013).
 - [12] J. Roslund, R. M. De Araújo, S. Jiang, C. Fabre, and N. Treps, Wavelength-multiplexed quantum networks with ultrafast frequency combs, *Nat. Photon.* **8**, 109 (2014).
 - [13] O. Pfister, Continuous-variable quantum computing in the quantum optical frequency comb, *J. Phys. B At. Mol. Opt. Phys.* **53**, 012001 (2020).
 - [14] Z. Yang, M. Jahanbozorgi, D. Jeong, S. Sun, O. Pfister, H. Lee, and X. Yi, A squeezed quantum microcomb on a chip, *Nat. Commun.* **12**, 4781 (2021).

- [15] J.-i. Yoshikawa, S. Yokoyama, T. Kaji, C. Sornphiphatphong, Y. Shiozawa, K. Makino, and A. Furusawa, Invited Article: Generation of one-million-mode continuous-variable cluster state by unlimited time-domain multiplexing, *APL Photon.* **1**, 060801 (2016).
- [16] M. V. Larsen, X. Guo, C. R. Breum, J. S. Neergaard-Nielsen, and U. L. Andersen, Deterministic generation of a two-dimensional cluster state, *Science* **366**, 369 (2019).
- [17] W. Asavanant, Y. Shiozawa, S. Yokoyama, B. Charoen-sombutamon, H. Emura, R. N. Alexander, S. Takeda, J. ichi Yoshikawa, N. C. Menicucci, H. Yonezawa, and A. Furusawa, Generation of time-domain-multiplexed two-dimensional cluster state, *Science* **366**, 373 (2019).
- [18] N. Huo, Y. Liu, J. Li, L. Cui, X. Chen, R. Palivel, T. Xie, X. Li, and Z. Y. Ou, Direct Temporal Mode Measurement for the Characterization of Temporally Multiplexed High Dimensional Quantum Entanglement in Continuous Variables, *Phys. Rev. Lett.* **124**, 213603 (2020).
- [19] J. Sun, W. Qu, E. Mikhailov, I. Novikova, H. Shen, and Y. Xiao, Spatial Multiplexing of Squeezed Light by Atomic Motion, *Phys. Rev. Lett.* **123**, 203604 (2018).
- [20] K. Zhang, W. Wang, S. Liu, X. Pan, J. Du, Y. Lou, S. Yu, S. Lv, N. Treps, C. Fabre, and J. Jing, Reconfigurable Hexapartite Entanglement by Spatially Multiplexed Four-Wave Mixing Processes, *Phys. Rev. Lett.* **124**, 090501 (2020).
- [21] X. Pan, S. Yu, Y. Zhou, K. Zhang, K. Zhang, S. Lv, S. Li, W. Wang, and J. Jing, Orbital-Angular-Momentum Multiplexed Continuous-Variable Entanglement from Four-Wave Mixing in Hot Atomic Vapor, *Phys. Rev. Lett.* **123**, 070506 (2019).
- [22] S. Li, X. Pan, Y. Ren, H. Liu, S. Yu, and J. Jing, Deterministic Generation of Orbital-Angular-Momentum Multiplexed Tripartite Entanglement, *Phys. Rev. Lett.* **124**, 083605 (2020).
- [23] N. Zhao, X. Li, G. Li, and J. M. Kahn, Capacity limits of spatially multiplexed free-space communication, *Nat. Photon.* **9**, 822 (2015).
- [24] E. Abramochkin and V. Volostnikov, Beam transformations and nontransformed beams, *Opt. Commun.* **83**, 123 (1991).
- [25] A. Forbes, M. de Oliveira, and M. R. Dennis, Structured light, *Nat. Photon.* **15**, 253 (2021).
- [26] M. A. Cox, L. Maqondo, R. Kara, G. Milione, L. Cheng, and A. Forbes, The resilience of Hermite-and Laguerre-Gaussian modes in turbulence, *J. Light. Technol.* **37**, 3911 (2019).
- [27] X. Gu, L. Chen, and M. Krenn, Phenomenology of complex structured light in turbulent air, *Opt. Express* **28**, 11033 (2020).
- [28] D. Aguirre-Olivas, G. Mellado-Villaseñor, V. Arrizón, and S. Chávez-Cerda, in *Laser Beam Shap. XVI*, Vol. 9581 (2015), p. 958105.
- [29] V. Delaubert, N. Treps, M. Lassen, C. C. Harb, C. Fabre, P. K. Lam, and H. A. Bachor, TEM10 homodyne detection as an optimal small-displacement and tilt-measurement scheme, *Phys. Rev. A* **74**, 053823 (2006).
- [30] B. K. Singh, H. Nagar, Y. Roichman, and A. Arie, Particle manipulation beyond the diffraction limit using structured super-oscillating light beams, *Light Sci. Appl.* **6**, e17050 (2017).
- [31] K. Wagner, J. Janousek, V. Delaubert, H. Zou, C. Harb, N. Treps, J. F. Morizur, K. L. Ping, and H. A. Bachor, Entangling the spatial properties of laser beams, *Science* **321**, 541 (2008).
- [32] C. Cai, L. Ma, J. Li, H. Guo, K. Liu, H. Sun, R. Yang, and J. Gao, Generation of a continuous-variable quadripartite cluster state multiplexed in the spatial domain, *Photon. Res.* **6**, 479 (2018).
- [33] X. F. Ren, G. P. Guo, J. Li, and G. C. Guo, Entanglement of the Hermite-Gaussian modes states of photons, *Phys. Lett. A* **341**, 81 (2005).
- [34] S. P. Walborn, S. Pádua, and C. H. Monken, Conservation and entanglement of Hermite-Gaussian modes in parametric down-conversion, *Phys. Rev. A* **71**, 053812 (2005).
- [35] J. Guo, C. Cai, L. Ma, K. Liu, H. Sun, and J. Gao, Higher order mode entanglement in a type II optical parametric oscillator, *Opt. Express* **25**, 4985 (2017).
- [36] V. Boyer, A. M. Marino, R. C. Pooser, and P. D. Lett, Entangled images from four-wave mixing, *Science* **321**, 544 (2008).
- [37] R. Simon, Peres-Horodecki Separability Criterion for Continuous Variable Systems, *Phys. Rev. Lett.* **84**, 2726 (2000).
- [38] M. Beijersbergen, L. Allen, H. van der Veen, and J. Woerdman, Astigmatic laser mode converters and transfer of orbital angular momentum, *Opt. Commun.* **96**, 123 (1993).
- [39] Y. Wang, Y. Chen, Y. Zhang, H. Chen, and S. Yu, Generalised Hermite-Gaussian beams and mode transformations, *J. Opt.* **18**, 055001 (2016).
- [40] N. Bozinovic, Y. Yue, Y. Ren, M. Tur, P. Kristensen, H. Huang, A. E. Willner, and S. Ramachandran, Terabit-scale orbital angular momentum mode division multiplexing in fibers, *Science* **340**, 1545 (2013).
- [41] W. N. Plick and M. Krenn, Physical meaning of the radial index of Laguerre-Gauss beams, *Phys. Rev. A* **92**, 063841 (2015).
- [42] G. Labroille, B. Denolle, P. Jian, P. Genevaux, N. Treps, and J.-F. Morizur, Efficient and mode selective spatial mode multiplexer based on multi-plane light conversion, *Opt. Express* **22**, 15599 (2014).
- [43] N. K. Fontaine, R. Ryf, H. Chen, D. Neilson, and J. Carpenter, in *2017 Eur. Conf. Opt. Commun.* (2017), p. 1.
- [44] Y. Zhou, J. Zhao, Z. Shi, S. M. Hashemi Rafsanjani, M. Mirhosseini, Z. Zhu, A. E. Willner, and R. W. Boyd, Hermite-Gaussian mode sorter, *Opt. Lett.* **43**, 5263 (2018).
- [45] N. Radwell, D. Brickus, T. W. Clark, and S. Franke-Arnold, High speed switching between arbitrary spatial light profiles, *Opt. Express* **22**, 12845 (2014).
- [46] B. Braverman, A. Skerjanc, N. Sullivan, and R. W. Boyd, Fast generation and detection of spatial modes of light using an acousto-optic modulator, *Opt. Express* **28**, 29112 (2020).
- [47] T. Sun, J. Kim, J. M. Yuk, A. Zettl, F. Wang, and C. Chang-hasnain, Surface-normal electro-optic spatial light modulator using graphene integrated on a high-contrast grating resonator, *Opt. Express* **24**, 26035 (2016).
- [48] A. Smolyaninov, A. El Amili, F. Vallini, S. Pappert, and Y. Fainman, Programmable plasmonic phase modulation of free-space wavefronts at gigahertz rates, *Nat. Photon.* **13**, 431 (2019).

- [49] B. C. dos Santos, K. Dechoum, and A. Z. Khoury, Continuous-Variable Hyperentanglement in a Parametric Oscillator with Orbital Angular Momentum, *Phys. Rev. Lett.* **103**, 230503 (2009).
- [50] K. Liu, J. Guo, C. Cai, S. Guo, and J. Gao, Experimental Generation of Continuous-Variable Hyperentanglement in an Optical Parametric Oscillator, *Phys. Rev. Lett.* **113**, 170501 (2014).
- [51] G. Ferrini, J. P. Gazeau, T. Coudreau, C. Fabre, and N. Treps, Compact Gaussian quantum computation by multi-pixel homodyne detection, *New J. Phys.* **15**, 093015 (2013).
- [52] Y. Cai, J. Roslund, G. Ferrini, F. Arzani, X. Xu, C. Fabre, and N. Treps, Multimode entanglement in reconfigurable graph states using optical frequency combs, *Nat. Commun.* **8**, 15645 (2017).